PUBLISHED VERSION

http://link.aps.org/doi/10.1103/PhysRevD.68.036003

http://hdl.handle.net/2440/11126

Meson model for $f_0(980)$ production in peripheral pion-nucleon reactions

F. P. Sassen, S. Krewald, and J. Speth

Institut für Kernphysik, Forschungszentrum Jülich GmbH, 52425 Jülich, Germany

A. W. Thomas

Special Research Centre for the Subatomic Structure of Matter, University of Adelaide, Adelaide 5005, Australia

The Jülich model for $\pi\pi$ scattering, based on an effective meson-meson Lagrangian, is applied to the analysis of the S-wave production amplitudes derived from the BNL E852 experiment $\pi^- p \to \pi^0 \pi^0 n$ for a pion momentum of 18.3 GeV and the GAMS experiments performed at 38 GeV and 100 GeV. The unexpected strong dependence of the S-wave partial wave amplitude on the momentum transfer between the proton and neutron in the vicinity of the $f_0(980)$ resonance is explained in our analysis as an interference effect between the resonance and the nonresonant background.

Meson spectroscopy in the scalar-isoscalar channel has received increasing interest motivated by the search for non-$q\bar{q}$ mesons, such as glueballs [1]. The large number of experimentally observed 0^{++} resonances suggests that some of those resonances may have a more complicated structure than the conventional $q\bar{q}$ structure [2,3]. The $f_0(980)$ has been a candidate for a non-$q\bar{q}$ meson for more than two decades [4–10].

Recently, the scalar-isoscalar $\pi\pi$ partial wave amplitudes have been deduced from two pion interaction obtained via the charge-exchange reaction $\pi^- p \to \pi^0 \pi^0 n$ measured for incident pion momentum of 18.3 GeV by the E852 Collaboration at the Brookhaven National Laboratory [11]. In the vicinity of the invariant two-pion mass $m_{\pi\pi} = 980$ MeV, a peculiar behavior of the S-wave amplitude has been observed. Such an effect has also previously been reported by the GAMS Collaboration for a beam momentum of 38 GeV [12]. While for small momentum transfers between the proton and the neutron ($-t < 0.1$ GeV^2) the scalar amplitudes show a dip around 1 GeV, a sharp peak is seen at the same energy for large momentum transfers ($-t > 0.4$ GeV^2).

This observation has been interpreted as evidence for a hard component in the $f_0(980)$ which would make the interpretation of this scalar meson as a $K\bar{K}$ molecule unconvincing [13–16]. Here we want to show that the strong dependence of the $f_0(980)$ production on the momentum transfer between the proton and the neutron is not in contradiction with a strong $K\bar{K}$ contribution to the $f_0(980)$. Actually we will show in the following that this t dependence is due to the interference between the resonance structure and the nonresonant background and does not depend on the detailed structure of the $f_0(980)$.

For ultrarelativistic beam momenta in the present kinematical regime the reaction $\pi^- p \to \pi^0 \pi^0 n$ is a peripheral one. This implies a relatively simple reaction mechanism which suppresses especially the excitation of nucleon resonances. The relevant Feynman diagrams are displayed in Fig. 1. In a peripheral reaction one assumes that the incoming pion interacts with the meson cloud of the proton only once. On the other hand one fully considers the final state

interaction between the produced mesons. In a peripheral charge-exchange reaction, only isovector mesons have to be considered. The ρ-meson cannot contribute because of G parity. This leaves the pion and the a_1-meson as the only relevant mesons with parity $P = (-1)^{J+1}$ to be exchanged in the t-channel. The a_2 for example cannot contribute in the reaction since it has quantum numbers $J^P = 2^+$. However the a_1-exchange is known to be important in peripheral πN-reactions [10,17].

The final state interaction of the produced mesons is described by an improved version of the Jülich meson-exchange model [6,18]. This means we use the Blankenbecler Sugar scattering equation [19] to generate our pion pion T-matrix.

$$T_{ij}(\vec{k}', \vec{k}; E) = V_{ij}(\vec{k}', \vec{k}; E) + \sum_l \int d^3 \vec{k}'' V_{il}(\vec{k}', \vec{k}''; E)$$
$$\times G_l(\vec{k}''; E) T_{lj}(\vec{k}'', \vec{k}; E).$$

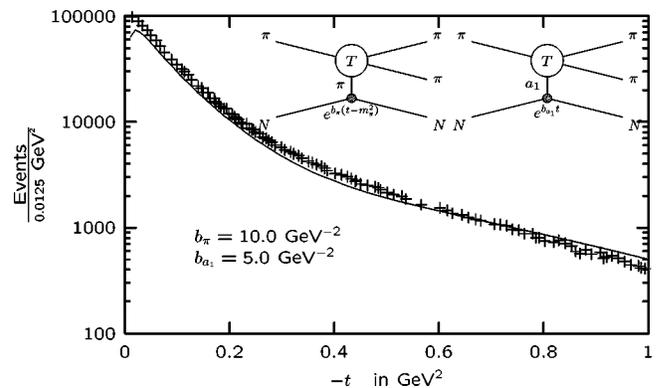Here $\vec{k}$ and $\vec{k}'$ are the momenta of the initial and final par-

FIG. 1. The $\pi^0 \pi^0$ production events as a function of the square t of the momentum transfer between proton and neutron. These data are used to determine the slope factors b. Solid line: meson-exchange model including final state interactions between the produced mesons (see Feynman diagrams of the inset). Crosses: the BNL-E852 data [11].

ticles in the center of mass frame and E is the total energy of the system. The propagator G has been constructed in a way that ensures unitarity for the S-matrix and is given by

$$G_l(\vec{k};E) = \frac{\omega_1(\vec{k}) + \omega_2(\vec{k})}{(2\pi)^3 2\omega_1(\vec{k})\omega_2(\vec{k})} \frac{1}{E^2 - [\omega_1(\vec{k}) + \omega_2(\vec{k})]^2}$$

with $\omega_{1/2}(\vec{k}) = \sqrt{\vec{k}^2 + m_{1/2}^2}$. Furthermore V is calculated in the one boson exchange approximation including s- and t-channel graphs. The subscripts to the transition matrix T, the propagator G and the potential V indicate the coupled channels used in our analysis. They are the $\pi\pi$ and the $K\bar{K}$ channel as well as the newly added πa_1 reaction channels. When adding the latter we used the Wess-Zumino Lagrangian [20] for the $a_1\rho\pi$-coupling.

We also investigated whether our $K\bar{K}$-molecule was artificially generated by the independent choice of s- and t-channel form factors. Correlating the form factors by dispersion relations we found no hint in this direction. In the original model, only one scalar meson $f_0(1400)$ was included. Now we consider both the $f_0(1370)$ and the $f_0(1500)$ mesons as s-channel diagrams. The couplings of these mesons to the three reaction channels considered were adjusted to reproduce the two-pion decays of the resonances. We found $g_{f_0(1370)K\bar{K}} = 0.551$, $g_{f_0(1370)\pi a_1} = 0.268$, and $g_{f_0(1500)\pi\pi} = g_{f_0(1500)K\bar{K}} = 0.188$. These are effective couplings which also simulate the influence of 4π decay channels. This is a minimal extension of the original Jülich model which allows to discuss the structure of the $f_0(980)$, which is our main point of interest. To analyze the decay structure of the $f_0(1370)$ and the $f_0(1500)$ mesons, the inclusion of 4π decays would be required, however [3]. The $\pi\pi$ phase shifts obtained in the new model are very similar to the ones of Ref. [6].

Given the large beam momentum, we describe the initial π- and a_1-meson exchanges by the corresponding Regge trajectories. In ultrarelativistic two-pion production reactions, the cross sections decrease exponentially with the momentum transfer t. In the partial wave analysis of the data, one therefore attaches a slope factor $e^{b_\pi(t - m_\pi^2)}$. The analysis of the BNL data required the introduction of two different slope factors. We interpret the two slope factors as effective form factors of the $pn\pi$- and the pna_1-vertices. Choosing $b_\pi = 10.0$ GeV^{-2} and $b_{a_1} = 5.0$ GeV^{-2}, the model can reproduce the experimental slope up to $-t = 2$ GeV^2, see Fig. 1. The full t-dependence is given by

$$\frac{\partial^2\sigma}{\partial m_{\pi\pi}\partial t} = A_\pi \frac{-t}{(t - m_\pi^2)^2} e^{b_\pi(t - m_\pi^2)} |T_{\pi\pi \to \pi\pi}(m_{\pi\pi},t)|^2$$

$$+ A_{a_1}(1 + tC)^2 e^{b_{a_1}t} |T_{\pi a_1 \to \pi\pi}(m_{\pi\pi},t)|^2. \quad (1)$$

Please note that A_π and A_{a_1} are not constant and that adding the absolute values squared is to account for the helicity structure as will be explained later. Furthermore C should be considered a free parameter as explained in [10] where our value of $C = -4.4$ GeV^2 was taken from.
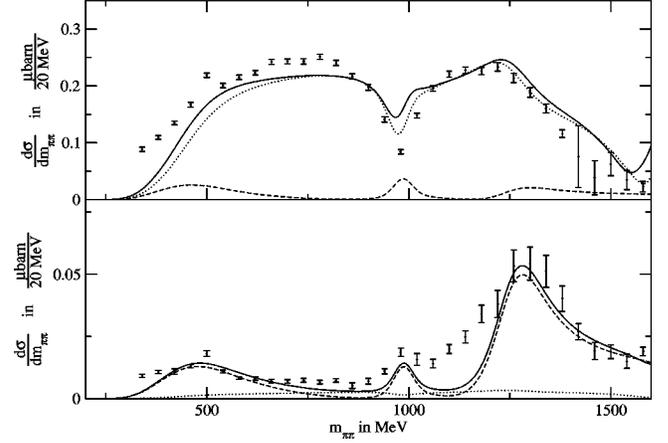

FIG. 2. The contribution of the S-wave to the total cross section is shown as a function of the invariant two-pion mass $m_{\pi\pi}$. Solid line: the meson-exchange model; dotted line: contribution generated by pion exchange at the proton-neutron vertex; dashed line: contribution generated by a_1 exchange at the proton-neutron vertex. In the upper part, the S-wave contributions to the cross section from [11] averaged for $0.01 < -t < 0.1$ GeV^2 are shown as a function of the invariant two pion mass, while in the lower part the corresponding data averaged for $0.4 < -t < 1.5$ GeV^2 are shown. The data are scaled according to the limits given in [21].

In Fig. 2, the S-wave contribution to the total cross section is shown as a function of the invariant two-pion mass. In the upper part, the data integrated over the momentum range $0.01 < -t < 0.1$ GeV^2 show a broad strength distribution from threshold to about 1.5 GeV, interrupted by a dip near 980 MeV. Our microscopic meson-theoretical model is able to reproduce this behavior nearly quantitatively. The model includes the $\pi\pi$, $K\bar{K}$, and πa_1 reaction channels, but no coupling to the $\rho\rho$-channel. For the small momentum transfers displayed in the upper part of Fig. 2, the contribution due to the exchange of a pion in the initial t-channel is dominant. For invariant masses $m_{\pi\pi}$ ranging from threshold to about 1 GeV, the experimental $\pi\pi$ phase shifts in the S-wave rise almost linearly to about 100°. The corresponding partial wave amplitude therefore becomes negative in the vicinity of $m_{\pi\pi} = 980$ MeV. This implies a destructive interference with the amplitude which describes the $f_0(980)$ meson and generates the dip seen in the data. At even higher energies the $f_0(1500)$ shows a similar behavior. At larger momentum transfers, the broad bump has disappeared in the data and one observes a narrow peak around 1 GeV. In that momentum regime (lower part of Fig. 2) the contribution due to the pion in the initial t-channel is negligibly small within our meson exchange model and the a_1 exchange gives the dominating contribution. (This can be traced back to the different slope factors.) Due to the spin structure, interference effects between a_1- and π-exchange can be neglected since the a_1-emission mainly conserves the helicity of the nucleon whereas the π-emission dominantly flips the nucleon helicity. But since the resonant contribution is now in phase with the nonresonant background we observe the opposite behavior compared to the upper part: the $f_0(980)$ resonance shows as a peak.
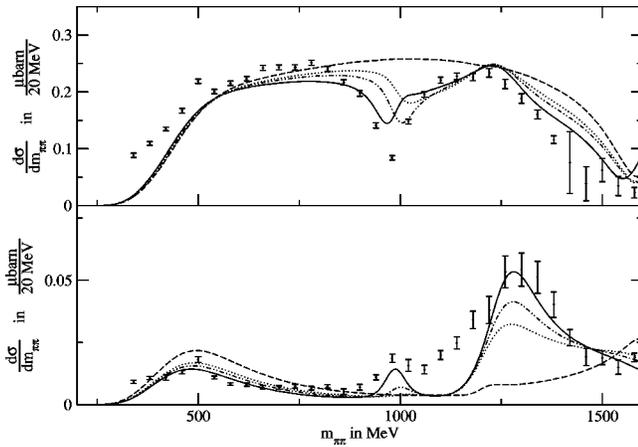
FIG. 3. The contribution of the S-wave to the total $\pi\pi$ cross section is shown as a function of the invariant two-pion mass $m_{\pi\pi}$. The transition potentials which couple to the $K\bar{K}$-channel via meson-exchanges in the t-channel are multiplied by a scaling factor, long-dashed: $\lambda = 0.0$, dotted: $\lambda = 0.75$, dash-dotted: $\lambda = 0.88$, solid: $\lambda = 1.0$. The data shown are taken from the BNL E852 Experiment [11]. The upper and lower part refer to small and large momentum transfers, as in Fig. 2.

In contrast to an empirical analysis which assumes a smooth background to which parametrized resonances are added [10,15], the present approach derives the background in a consistent way within our model. This is essential for interference effects. To illustrate this point, we performed a series of calculations in which the transition potentials connecting the $\pi\pi$ channel and the $K\bar{K}$ channel via t-channel meson exchanges were multiplied by a scaling factor λ which we changed from 0 to 1. The t-channel meson exchanges within the $K\bar{K}$ channel were scaled by the same factor. For $\lambda = 0$, the $\pi\pi$ and $K\bar{K}$ channel can interact only via s-channel diagrams. The corresponding contributions to the S-wave total cross sections are shown in Fig. 3.

For small momentum transfers t between the proton and the neutron (upper part of Fig. 3), one finds a broad strength distribution extending up to 1500 MeV, if the t-channel coupling to the $K\bar{K}$ channel is switched off ($\lambda = 0$). Allowing a small coupling to the $K\bar{K}$ channel ($\lambda = 0.75$), the cross section decreases in the energy region between 1000 MeV and the onset of the $f_0(1370)$ resonance at about 1250 MeV. As the scaling strength λ is further increased, a dip develops near $m_{\pi\pi} = 980$ MeV. For large momentum transfers t between the proton and the neutron (lower part of Fig. 3), a bump in the vicinity of $m_{\pi\pi} = 980$ MeV appears when the coupling to the $K\bar{K}$ channel is switched on.

Near $m_{\pi\pi} = 500$ MeV, a calculation without coupling to the $K\bar{K}$ channel overestimates the data. With increasing coupling strength λ the shape of the experimental strength distribution and the relative size of the bumps centered at $m_{\pi\pi} = 500$ MeV and $m_{\pi\pi} = 980$ MeV are reproduced. It is important to realize that this feature emerges in a natural way from a model for the $\pi\pi$ phase shifts when proper Regge production amplitudes are used. Here for example the $(1 + tC)^2$ part of Eq. (1), which already appears in early
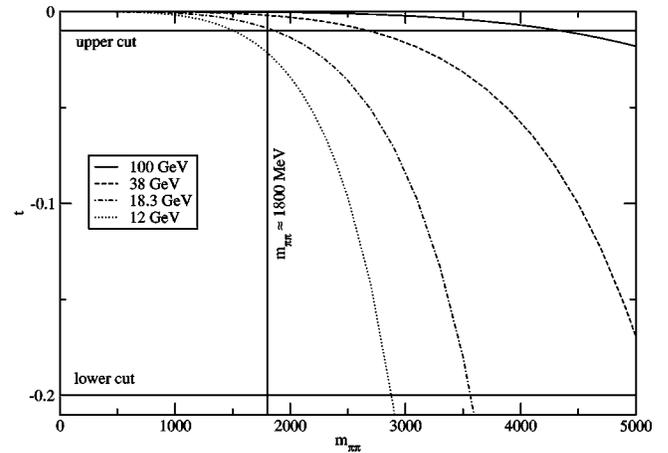

FIG. 4. The upper kinematic limit of t is plotted against the invariant mass of the two pion system $m_{\pi\pi}$ for four different beam energies corresponding to GAMS 100 GeV, GAMS 38 GeV, BNL 18.3 GeV and KEK 12 GeV. For comparison also the upper and lower limit applied in the experimental low momentum transfer cut are shown.

analysis of $\pi N \rightarrow \pi\pi N$ scattering data e.g. [22], is essential to the low energy part of the high momentum transfer case.

One should further notice that a cross check with data from other experiments with different t-binning and beam energy is of course interesting but can only contribute limited information in our case. To arrive at this conclusion let us have a look at the influence of the beam energy on the production. Firstly the beam energy enters as a factor of $1/q^2_{beam}s_{tot}$, which cannot be observed by us, since the data are not normalized. Secondly it enters by limiting the range of the t-integration. This is shown in Fig. 4 for several beam energies together with the cut ($0.01 < -t < 0.2$) applied to the momentum transfer in the analysis. One observes that for the beam energies for which experimental data are available, the limits on t are essentially determined by the analysis and not by kinematics if one looks at invariant two pion masses below ≈ 1800 MeV. This is strictly true for the data under consideration here since we do not consider the 12 GeV KEK data which are only available as an extrapolation to the pion pole. This means that below an invariant two pion mass of 1800 MeV the data sets should be identical up to an overall scaling.

The invariant mass range to which our model is applicable extends up to at most 1.5 GeV. This means that the sets of data stemming from different beam energies should be identical in our invariant mass region of interest. Thus we compare the two sets of GAMS data at 38 GeV and at 100 GeV and the 18.3 GeV BNL data as is shown in Fig. 5. The upper panel shows the BNL data (filled circles) together with the GAMS data at 100 GeV (crosses) and at 38 GeV (open squares) for the low momentum transfer case $0.01 < -t < 0.20$ GeV^2. We see that the data sets and our calculations are up to scaling in good agreement. Only the GAMS 38 GeV data deviate in shape from the other two data sets in the invariant two pion mass region 0.8–1.0 GeV and above 1.2 GeV.
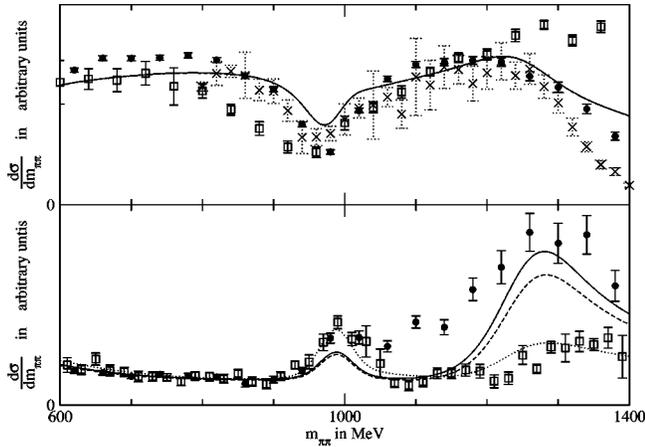
FIG. 5. The contribution of the *S*-wave to the total $\pi\pi$ cross section is shown as a function of the invariant two-pion mass $m_{\pi\pi}$. The upper panel shows our prediction for $0.01 < -t < 0.20$ GeV^2 together with experimental data from different beam energies. Crosses: 100 GeV GAMS [23], squares: 38 GeV GAMS [12], circles: 18.3 GeV BNL [11]. The lower panel compares two *t*-ranges and our corresponding predictions: Circles and solid line: $0.3 < -t < 1.5$ GeV^2 [11]; squares and interrupted lines: $0.3 < -t < 1.0$ GeV^2 [12]. The dashed line is the original model, the dotted line shows a calculation with $f_0(1370)$ couplings adjusted to the GAMS data.

FIG. 6. The contribution of the *S*-wave to the total cross section is shown as a function of the invariant two-pion mass $m_{\pi\pi}$. Both panels show the BNL data (circle) [11] and the GAMS data (squares) [12]. The GAMS data have been derived as the difference of two data sets and errors have been scaled down by a factor of four to guide the eye. The curves show the results of our calculation (solid line) and of a model with the $f_0(1370)$ coupling taken from the GAMS case in Fig. 5 (dotted line). The upper panel shows momentum transfers $0.3 < -t < 0.4$ GeV^2 and the lower panel momentum transfers $0.2 < -t < 0.4$ GeV^2 (no data available from GAMS).

Comparing the sets of data in the case of high momentum transfer is not that easy since BNL only quotes a *t*-binning of $0.4 < -t < 1.5$ GeV^2 whereas GAMS quotes $0.3 < -t < 1.0$ GeV^2. Nevertheless a comparison might be more rewarding since looking at different *t*-binning means looking at a different ratio of the two production mechanisms. To have at least a common upper limit we join bins for the BNL case to get a momentum transfer range of $0.3 < -t < 1.5$ GeV^2 and plotted it together with the GAMS $0.3 < -t < 1.0$ GeV^2 data and our calculations for both *t*-ranges. Having a common upper limit and knowing that production mainly takes place at low absolute momentum transfers $|t|$ makes this approach justifiable. This comparison is shown in the lower panel of Fig. 5. The data coincide up to 1.05 GeV, at which point they start to deviate strongly. It is tempting to assign the difference to the production in the momentum transfer range $1.0 < -t < 1.5$ GeV^2 and to interpret this as the $f_0(1370)$ being a very compact object which can be produced at large momentum transfers. Our calculation shows a different behavior: The BNL data are reasonably well described (solid curve compared to circles), but our model predicts a much too strong production above 1.05 GeV in the case of the GAMS data. The dashed line is our prediction in the case of the GAMS data which are shown as squares. In the following section we will point out that the BNL and GAMS data are inconsistent and that we are not in a position to judge which one is correct so we also introduce a fit to the GAMS data (dotted line) by just varying the coupling of the πa_1-channel to the $f_0(1370)$ and thus not changing the low momentum transfer behavior. The good agreement of this second fit to the GAMS data also at other momentum transfers (as can be seen in Fig. 6) demonstrates that our conclu-
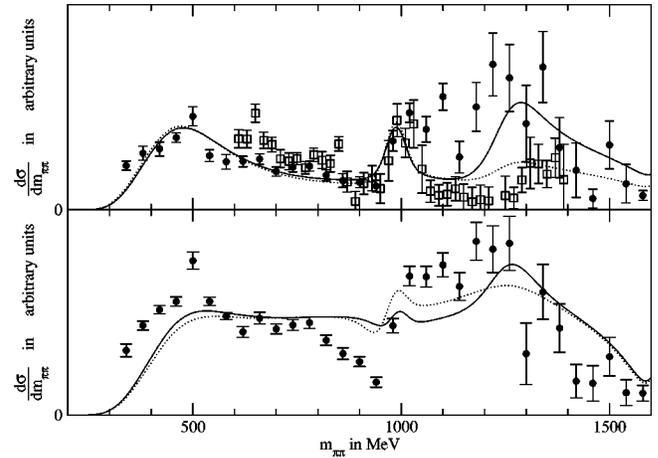
sions on the $K\bar{K}$ contribution to the $f_0(980)$ stand firm for both sets of data but only the parameters for the admixture of the $f_0(1370)$ need to be questioned.

To come to the conclusion that the GAMS and BNL data are inconsistent we looked at the highest momentum transfer range where data from both GAMS and BNL are available, $0.3 < -t < 0.4$ GeV^2. We show these data in the upper panel of Fig. 6. The GAMS data needed to be derived from the data published in [12] by subtracting two sets of data. The resulting errors have been scaled down by a factor of four so that the errors shown here roughly correspond to the spreading of the data. We believe this to be a more realistic estimate of the error. Already at this momentum transfer range the two sets of data start to deviate in shape at about 1.05 GeV even though they should be identical up to a scaling factor. Our calculation again reproduces the BNL data whereas the GAMS data are overestimated. When using the coupling parameter for the $f_0(1370)$ which has been fitted against the high momentum data of GAMS (dotted lines in Figs. 5 and 6) instead of the parameter fitted to the BNL data a good description is achieved, however we find that our model reproduces the *t*-dependence in the data very well, both if we look at the BNL data only or at the GAMS data only. Of course we cannot resolve the discrepancy between the two data sets.

A comparison of our model to the intermediate *t*-range is problematic since our predictions in this case are very sensitive to the slope parameters for π and a_1 exchange, which in turn cannot be fixed to a sufficient accuracy by the fit to the $d\sigma/dt$ plot. This problem arises because our predictions strongly depend on the point where the production mechanisms become equally important and this point changes rap-

idly with the slope parameters. Fitting the data in this case would mean stronger fine tuning of the parameters than would be appropriate for a microscopic model like ours. In the lower panel of Fig. 6 we nevertheless show our results for this momentum transfer range ($0.2 < -t < 0.4$ GeV^2). In order to demonstrate that there is also a strong variation with the coupling to the $f_0(1370)$ we show both the calculation with an $f_0(1370)$ as demanded by the BNL data (solid line) as well as the calculation with the $f_0(1370)$ which has been fitted to the GAMS data (dotted line). Even though there are no GAMS data available in this momentum transfer range we can infer from the data shown in the upper panel in Fig. 6, which displays a subset of the t-range shown the lower panel, that above 1.05 GeV invariant two pion mass the data points of the GAMS experiment should be lower than the BNL data. Keeping in mind which size of discrepancies has to be expected between the different experiments we conclude that even for the medium momentum transfer range our calculation reproduces the main features of the data as well as one might expect from a microscopic model like ours.

Finally, we compare the results of our model for the reaction $\pi^- p \rightarrow K^0 \bar{K}^0 n$ with the published data [24]. The model works satisfactorily from threshold up to about 1200 MeV. Beyond that energy, our model strongly overestimates the production of neutral kaons (dashed line in Fig. 7). This is understood when comparing our effective couplings to the decays of the $f_0(1370)$ and $f_0(1500)$ resonances as listed in [25]. We used a strong coupling to the $K\bar{K}$ to simulate decays which in reality go to 4π-channels thus naturally overestimating the kaon production. The solid line in Fig. 7 shows a version of the model where this shortcoming has been removed by a mock $\sigma\sigma$-channel to account for
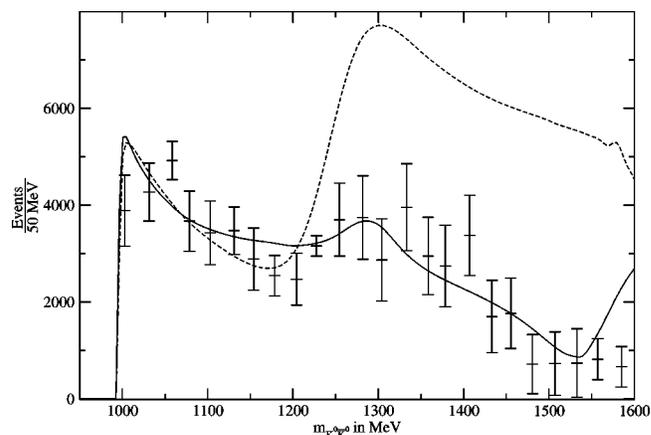

FIG. 7. The contribution of the S-wave to the production $\pi^- p \rightarrow K^0 \bar{K}^0 n$ is shown as a function of the invariant two-kaon mass $m_{K\bar{K}}$. Dashed: our model with overestimation due to missing 4π-decays, solid: model with additional $\sigma\sigma$-channel. The data shown are taken from [24] with the bin width of 50 MeV not shown.

4π-decays. A good description of the data is obtained even beyond 1200 MeV where the partial wave amplitudes are strongly dominated by resonances.

We conclude that the Jülich model which predicts a strong $K\bar{K}$ molecule contribution in the $f_0(980)$ can explain the strong dependence of the S-wave production on the momentum transfer between the proton and the neutron near $m_{\pi\pi} = 980$ MeV by an interference mechanism.

[1] C. Amsler, Rev. Mod. Phys. **70**, 1293 (1998).

[2] C. Amsler, Phys. Lett. B **541**, 22 (2002).

[3] Crystal Barrel Collaboration, A. Abele *et al.*, Eur. Phys. J. C **21**, 261 (2001).

[4] R.L. Jaffe, Phys. Rev. D **15**, 267 (1977).

[5] J.D. Weinstein and N. Isgur, Phys. Rev. D **41**, 2236 (1990).

[6] D. Lohse, J.W. Durso, K. Holinde, and J. Speth, Nucl. Phys. **A516**, 513 (1990).

[7] T. Barnes, Phys. Lett. **165B**, 434 (1985).

[8] M.A. Pichowsky, A. Szczepaniak, and J.T. Londergan, Phys. Rev. D **64**, 036009 (2001).

[9] J.A. Oller, E. Oset, and J.R. Pelaez, Phys. Rev. Lett. **80**, 3452 (1998).

[10] N.N. Achasov and G.N. Shestakov, Phys. Rev. D **58**, 054011 (1998).

[11] E852 Collaboration, J. Gunter *et al.*, Phys. Rev. D **64**, 072003 (2001).

[12] GAMS Collaboration, D. Alde *et al.*, Z. Phys. C **66**, 375 (1995).

[13] E. Klempt, hep-ex/0101031.

[14] A.A. Kondashov, Nucl. Phys. B (Proc. Suppl.) **74**, 180 (1999).

[15] V.V. Anisovich, A.V. Sarantsev, A.A. Kondashov, Y.D. Prokoshkin, and S.A. Sadovsky, Phys. Lett. B **355**, 363 (1995).

[16] V.V. Anisovich, hep-ph/0208123.

[17] R. Kaminski, L. Lesniak, and B. Loiseau, Phys. Lett. B **413**, 130 (1997).

[18] O. Krehl, R. Rapp, and J. Speth, Phys. Lett. B **390**, 23 (1997).

[19] R. Blankenbecler and R. Sugar, Phys. Rev. **142**, 1051 (1966).

[20] J. Wess and B. Zumino, Phys. Rev. **163**, 1727 (1967).

[21] R. Kaminski, L. Lesniak, and K. Rybicki, EPJdirect C **4**, 4 (2002).

[22] J. Kimel and J. Owens, Nucl. Phys. **B122**, 464 (1977).

[23] GAMS Collaboration, D. Alde *et al.*, Eur. Phys. J. A **3**, 361 (1998).

[24] A. Etkin *et al.*, Phys. Rev. D **25**, 1786 (1982).

[25] Particle Data Group, K. Hagiwara *et al.*, Phys. Rev. D **66**, 010001 (2002).